Voltage-induced Wrinkling in a Constrained Annular Dielectric Elastomer Film

Kai Li,[1] Wanfang Wu,[2] Ziyang Jiang,[2] Shengqiang Cai*[2]

[1]*Department of Civil Engineering, Anhui Jianzhu University, Hefei, Anhui 230601, P R China*

[2]*Department of Mechanical and Aerospace Engineering, University of California, San Diego La Jolla, CA 92093, USA*

Abstract

Wrinkles can be often observed in dielectric elastomer (DE) films when they are subjected to electrical voltage and mechanical forces. In the applications of DEs, wrinkle formation is often regarded as an indication of system failure. However, in some scenarios, wrinkling in DE does not necessarily result in material failure and can be even controllable. Although tremendous efforts have been made to analyze and calculate a variety of deformation modes in DE structures and devices, a model which is capable of analyzing wrinkling phenomena including the critical electromechanical conditions for the onset of wrinkles and wrinkle morphology in DE structures is currently unavailable. In this paper, we experimentally demonstrate controllable wrinkling in annular DE films with the central part being mechanically constrained. By changing the ratio between the inner radius and outer radius of the annular films, wrinkles with different wavelength can be induced in the films when externally applied voltage exceeds a critical value. To analyze wrinkling phenomena in DE films, we formulate a linear plate theory of DE films subjected to electromechanical loadings. Using the model, we successfully predict the wavelength

of the voltage-induced wrinkles in annular DE films. The model developed in this article can be used to design voltage-induced wrinkling in DE structures for different engineering applications.

Keywords

Dielectric elastomer; Wrinkling; Annular film; Linear plate theory; Linear stability analysis

---

*E-mail address of the corresponding author: shqcai@ucsd.edu

1. Introduction

A dielectric elastomer (DE) can deform when it is under the action of electrical field or mechanical forces. Because of the advantages of easy fabrication, low cost, excellent deformability and electromechanical robustness, DEs have been recently intensively explored and developed to a variety of structures with diverse functions (Carpi et al., 2008; O' Halloran et al., 2008). For instance, DE films with different shapes and sizes have been fabricated to harvest energy from different sources such as ocean wave (Kornbluh et al., 2012b), motions of human-beings, wind and even combustion (Kornbluh et al., 2012a). DEs have also been used as artificial muscles in designing walking robots (Brochu and Pei, 2010), programmable grippers (Shian et al., 2015), camouflage devices (Wang et al., 2014) and antifouling systems (Shivapooja et al., 2013). In addition to those, transparent DE loudspeakers (Keplinger et al., 2013), planar DE rotary motors (Anderson et al., 2010) and nonlinear DE strain gauges (Xu et al., 2015) have also been successfully made recently.

In most of the applications, large deformation in DEs can be ubiquitously observed. General three dimensional models for the finite deformation of DEs under the actions of an arbitrary field of electrical potential and forces have been formulated by different researchers (Dorfman and Ogden, 2005; Goulbourne et al., 2005; McMeeking and Landis, 2005; Vu et al., 2007; Suo et al., 2008; O'Brien et al., 2009; Trimarco, 2009). Numerous phenomena associated with the electro-mechanical coupling in DEs have been successfully analyzed using these

developed models, such as the pull-in instability in a DE membrane sandwiched by two compliant electrodes (Zhao and Suo, 2007; Norris, 2008; Zhou et al., 2008), voltage-induced creasing and cratering instabilities in a constrained DE layer (Wang et al., 2011), giant deformation and shape bifurcation in DE balloons (Li et al., 2013; Liang and Cai, 2015), and instabilities in layered soft dielectrics (Bertoldi and Gei, 2011; Dorfmann and Ogden, 2014).

Because large deformation in a DE requires relatively large electric field, thin DE films are frequently adopted in most applications. As a consequence, multiple wrinkles can be often observed in the experiments in DE structures when they are subjected to electromechanical loading. Wrinkle formation has been often regarded as one of the failure mechanisms in DE devices (Plante and Dubowsky, 2006; De Tommasi et al., 2011; De Tommasi et al., 2013a; De Tommasi et al., 2013b; Zurlo, 2013; De Tommasi et al., 2014). In the last few years, it has been shown that in certain conditions, wrinkle formation in DE structures can be reversible and leads to no damage of the material (Plante and Dubowsky, 2006; Kollosche et al. 2015; Lu et al., 2015; Mao et al., 2015; Liu et al., 2016). Moreover, the wrinkles in DE structures may provide additional functions which cannot be easily obtained otherwise.

To predict the critical conditions of wrinkling in a DE film under different electromechanical loading, the film is usually assumed to be under plane stress condition. Because DE films are thin and can bear little compression, the external electromechanical loading which leads to the loss of tension at any point of the DE film is commonly adopted to represent the critical condition for the wrinkle

formation (Huang and Suo, 2012; Park et al., 2012; Zhu et al., 2012; Díaz-Calleja et al., 2013; Díaz-Calleja et al., 2014) or failure of the structure. Reasonable agreements between the predictions and experimental measurements of the conditions for the onset of wrinkles in DE membranes have been obtained in several different studies (Conn et al., 2012; Zhu et al., 2012; Kollosche et al. 2015; Xie et al., 2016).

Nevertheless, though the loss of tension can be used to estimate the critical conditions for the wrinkle formation in a DE film, analyses based on plane stress assumption cannot provide additional information about wrinkle morphology such as wavelength of wrinkles. Considering the recent interests in harnessing instabilities of soft active structures to achieve novel functions, a theoretical method which can accurately predict the critical conditions of wrinkling and the morphology of wrinkles in a DE film subjected electromechanical loading is highly desired.

Most current electromechanical constitutive models of DE films are based on membrane assumption. Specifically, stress in a DE film is assumed to be uniform along its thickness direction and its bending stiffness is completely ignored. Such assumptions greatly simplify the way of computing stress/stretch field and electrical field in DE structures under different loading conditions. The computational results based on the membrane assumption often agree well with experiments. However, the onset of wrinkles in a film is a result of competition between its bending energy and stretching energy. Therefore, taking account of the bending energy of a DE film becomes critical in analyzing the wrinkle formation and its morphology.

A general formulation of plate theory for DE films subjected to electromechanical loading is extremely challenging, which mainly stem from large deformation of the material, coupling between mechanics and electrical field, and complex geometries. To develop a model for predicting the critical condition of wrinkling instability, instead of establishing a general plate theory for DE thin films, we analyze the problem with a small three dimensional displacement field associated with bending deformation superposed onto a finite 2D deformation state of a DE film. Because the additional three dimensional displacement field is small and we only focus on the bending of the DE film, we prescribe the form of additional displacement field by following Kirchhoff assumptions of linear plate theory. In addition, because the thickness of the DE film is unchanged with the additional superposed displacement field, Maxwell stress in the DE film is assumed to remain the same.

Wrinkling in an annular membrane, caused by surface tension (Piñeirua et al. 2013), inhomogeneous growth (Mora and Boudaoud, 2006; Dervaux and Amar, 2008), mechanical force (Coman and Bassom, 2007; Davidovitch et al., 2011), has been intensively studied in the past. As a demonstration of the application of our model, in this paper, we analyze the wrinkle formation in an annular DE film with internal constraint as shown in Fig. 1. It is easy to show that the model developed below can be directly applied to analyzing wrinkling in DE films with different geometries and under arbitrary electromechanical loadings.

2. Experiment

In the experiment, we use laser cutter to cut a circular DE film (VHB 4905 purchased from 3M company), and paint carbon grease on both surfaces of the DE film as compliant electrode. To avoid electrical arcing across free edge of the film, we intentionally leave an annular gap near the edge of the film unpainted as shown in Fig. 1. We next glue a circular acrylate plate with different diameters on the center of the DE film to constrain its deformation. The adhesion between VHB film and the acrylate plate is strong enough and no debonding and sliding has been observed in our experiments. Finally, we apply an electrical voltage across the thickness of the annular DE film with gradually increasing the magnitude. When the voltage is high enough, wrinkles can be clearly observed in the film. Depending on the size of the central rigid plate, wrinkles with different wavelength may appear as shown in Fig. 1. If the voltage in the experiments is not too high, the formation and annihilation of wrinkles can repeat many times with the voltage being turned on and off.

3. Model and formulation

3.1 A constrained annular DE film subjected to an electrical voltage

Fig. 2 sketches an annular DE film with clamped inner boundary. In the undeformed state, the thickness of the film is denoted by H. The inner radius and outer radius of the annular plate are denoted by A and B, respectively. In the actuated state, a voltage Φ is applied between the two surfaces of the film. When the voltage is small, the DE film deforms axisymmetrically and maintains flat configuration (Fig. 2b). The hoop stress in the DE film is compressive while the radial

stress is always tensile. With increasing the voltage, the compressive hoop stress increases and finally wrinkles form in the DE film as shown in Fig. 1 and Fig. 2c. In the following, we first analyze the deformation of DE film without wrinkles.

In the reference state, we label each material particle by its radial coordinate R in the interval (A,B). In a deformed state, the material particle R takes the position of coordinate $r(R)$. The function $r(R)$ describes the deformed state of the DE film. The radial stretch and the hoop stretch can be calculated as

$$\lambda_r = \frac{dr}{dR}, \tag{1}$$

$$\lambda_\theta = \frac{r}{R}. \tag{2}$$

The DE is assumed to be incompressible, so that the stretch in thickness direction is $\lambda_z = 1/\lambda_r\lambda_\theta$.

The electrical field E in the DE film is along the normal direction of the film and relates to the voltage Φ as

$$E = \frac{\Phi}{h}, \tag{3}$$

where h is the thickness of the film in the deformed state, so $h = H\lambda_z$.

The equation of force balance in the annular DE film is given by

$$\frac{d}{dR}\left(\frac{\sigma_{rr}}{\lambda_r}\right) - \frac{1}{R}\left(\frac{\sigma_{\theta\theta}}{\lambda_\theta} - \frac{\sigma_{rr}}{\lambda_r}\right) = 0. \tag{4}$$

In the paper, we adopt ideal dielectric elastomer model, which assumes electrical

permittivity is a constant and unaffected by the deformation and electrical field (Suo et al., 2008). Meanwhile, neo-Hookean model is adopted here to describe the hyperelasticity of the material. As a consequence, we have the following constitutive equation:

$$\sigma_{rr} = \mu\left(\lambda_r^2 - \lambda_r^{-2}\lambda_\theta^{-2}\right) - \varepsilon E^2, \tag{5}$$

$$\sigma_{\theta\theta} = \mu\left(\lambda_\theta^2 - \lambda_r^{-2}\lambda_\theta^{-2}\right) - \varepsilon E^2, \tag{6}$$

where the first term in the above two equations originates from the elasticity of the elastomer and the second term is known as Maxwell stress.

From the equilibrium Eq. (4), we can obtain the first derivative of $\lambda_r(R)$:

$$\frac{d\lambda_r}{dR} = \frac{\dfrac{\sigma_{\theta\theta}}{\lambda_\theta} - \dfrac{\sigma_{rr}}{\lambda_r} + \left(\lambda_\theta - \lambda_r\right)\dfrac{\partial}{\partial\lambda_\theta}\left(\dfrac{\sigma_{rr}}{\lambda_r}\right)}{R\dfrac{\partial}{\partial\lambda_r}\left(\dfrac{\sigma_{rr}}{\lambda_r}\right)}. \tag{7}$$

First derivative of $\lambda_\theta(R)$ in Eq. (2) gives that

$$\frac{d\lambda_\theta}{dR} = \frac{\lambda_r - \lambda_\theta}{R}. \tag{8}$$

The ordinary differential equations (ODEs) of (7) and (8) can be solved numerically with the following two boundary conditions:

$$r(A) = A, \tag{9}$$

$$\sigma_{rr}(B) = 0. \tag{10}$$

3.2 Linear stability analysis of voltage-induced wrinkles in a DE film

As discussed above, voltage-induced compressive hoop stress in the annular DE film may result in wrinkling. To investigate the formation and morphology of wrinkles, we first formulate a linear plate theory for a DE film under electromechanical loading.

To derive the governing equations for the deflection of a DE film, we first need to obtain the relationship between the stress and deflection of the film subjected electromechanical loadings. For the purpose of clarity and simplicity, we first derive the stress-deflection relationship of a DE film in a Cartesian coordinate, and then we transfer the results to a polar coordinate.

We consider an element of a DE film subjected to a homogeneous electrical field along the thickness direction. The deformation gradient of the film from initial undeformed state denoted by $\mathbf{B}_i$ to a flat state denoted by $\mathbf{B}_o$ is given by

$$\mathbf{F}_0 = \begin{bmatrix} \lambda_x & 0 & 0 \\ 0 & \lambda_y & 0 \\ 0 & 0 & \lambda_z \end{bmatrix}, \tag{11}$$

where λ_x, λ_y and λ_z are principle stretches in three orthogonal directions x, y and z, where x and y are two perpendicular directions in the plane of the film, and z is the direction perpendicular to the film.

Next, we assume the displacement field associated with wrinkling deformation can be represented by u, v and w in the three orthogonal directions x, y and z. The deformation gradient from the predeformed state $\mathbf{B}_o$ to wrinkled state $\mathbf{B}_1$ can be given by

$$\mathbf{F}_1 = \begin{bmatrix} 1+\dfrac{\partial u}{\partial x} & \dfrac{\partial u}{\partial y} & \dfrac{\partial u}{\partial z} \\ \dfrac{\partial v}{\partial x} & 1+\dfrac{\partial v}{\partial y} & \dfrac{\partial v}{\partial z} \\ \dfrac{\partial w}{\partial x} & \dfrac{\partial w}{\partial y} & 1+\dfrac{\partial w}{\partial z} \end{bmatrix}. \tag{12}$$

Therefore, the deformation gradient from initial state $\mathbf{B}_i$ to wrinkled state $\mathbf{B}_1$ can be calculated as

$$\mathbf{F} = \mathbf{F}_1 \cdot \mathbf{F}_0 = \begin{bmatrix} \lambda_x\left(1+\dfrac{\partial u}{\partial x}\right) & \lambda_y \dfrac{\partial u}{\partial y} & \lambda_z \dfrac{\partial u}{\partial z} \\ \lambda_x \dfrac{\partial v}{\partial x} & \lambda_y\left(1+\dfrac{\partial v}{\partial y}\right) & \lambda_z \dfrac{\partial v}{\partial z} \\ \lambda_x \dfrac{\partial w}{\partial x} & \lambda_y \dfrac{\partial w}{\partial y} & \lambda_z\left(1+\dfrac{\partial w}{\partial z}\right) \end{bmatrix}. \tag{13}$$

The corresponding left Cauchy-Green strain tensor is

$$\mathbf{B} = \mathbf{F} \cdot \mathbf{F}^{\mathrm{T}} = \begin{bmatrix} \lambda_x^2\left(1+2\dfrac{\partial u}{\partial x}\right) & \lambda_x^2 \dfrac{\partial v}{\partial x} + \lambda_y^2 \dfrac{\partial u}{\partial y} & \lambda_x^2 \dfrac{\partial w}{\partial x} + \lambda_z^2 \dfrac{\partial u}{\partial z} \\ \lambda_x^2 \dfrac{\partial v}{\partial x} + \lambda_y^2 \dfrac{\partial u}{\partial y} & \lambda_y^2\left(1+2\dfrac{\partial v}{\partial y}\right) & \lambda_y^2 \dfrac{\partial w}{\partial y} + \lambda_z^2 \dfrac{\partial v}{\partial z} \\ \lambda_x^2 \dfrac{\partial w}{\partial x} + \lambda_z^2 \dfrac{\partial u}{\partial z} & \lambda_y^2 \dfrac{\partial w}{\partial y} + \lambda_z^2 \dfrac{\partial v}{\partial z} & \lambda_z^2\left(1+2\dfrac{\partial w}{\partial z}\right) \end{bmatrix}. \tag{14}$$

Based on ideal dielectric elastomer model, Cauchy stress in a DE film can be decomposed into elastic part and Maxwell stress, namely,

$$\boldsymbol{\sigma} = \boldsymbol{\sigma}_{\mathrm{ela}} + \boldsymbol{\sigma}_{\mathrm{m}}, \tag{15}$$

where Maxwell stress is a tensor and can be represented by

$$\boldsymbol{\sigma}_{\mathrm{m}}=\begin{bmatrix}-\frac{1}{2}\varepsilon E^{2} & 0 & 0\\ 0 & -\frac{1}{2}\varepsilon E^{2} & 0\\ 0 & 0 & \frac{1}{2}\varepsilon E^{2}\end{bmatrix}, \tag{16}$$

and elastic stress $\boldsymbol{\sigma}_{\mathrm{ela}}$ is given by

$$\boldsymbol{\sigma}_{\mathrm{ela}}=\mathbf{F}\frac{\partial W_{\mathrm{stretch}}}{\partial \mathbf{F}}-p\mathbf{I}\,, \tag{17}$$

where W_{stretch} is strain energy density of the elastomer and p is hydrostatic pressure for the incompressibility of the elastomer. We adopt neo-Hookean model in the current article, so Eq. (17) can be written explicitly as

$$\boldsymbol{\sigma}_{\mathrm{ela}}=\mu\mathbf{B}-p\mathbf{I}\quad. \tag{18}$$

Inserting Eqs. (18) and (16) into (15) leads to

$$\boldsymbol{\sigma}=\begin{bmatrix}-p-\frac{\varepsilon E^{2}}{2}+\mu\lambda_{x}^{2}\left(1+2\frac{\partial u}{\partial x}\right) & \mu\left(\lambda_{x}^{2}\frac{\partial v}{\partial x}+\lambda_{y}^{2}\frac{\partial u}{\partial y}\right) & \mu\left(\lambda_{x}^{2}\frac{\partial w}{\partial x}+\lambda_{z}^{2}\frac{\partial u}{\partial z}\right)\\ \mu\left(\lambda_{x}^{2}\frac{\partial v}{\partial x}+\lambda_{y}^{2}\frac{\partial u}{\partial y}\right) & -p-\frac{\varepsilon E^{2}}{2}+\mu\lambda_{y}^{2}\left(1+2\frac{\partial v}{\partial y}\right) & \mu\left(\lambda_{y}^{2}\frac{\partial w}{\partial y}+\lambda_{z}^{2}\frac{\partial v}{\partial z}\right)\\ \mu\left(\lambda_{x}^{2}\frac{\partial w}{\partial x}+\lambda_{z}^{2}\frac{\partial u}{\partial z}\right) & \mu\left(\lambda_{y}^{2}\frac{\partial w}{\partial y}+\lambda_{z}^{2}\frac{\partial v}{\partial z}\right) & -p+\frac{\varepsilon E^{2}}{2}+\mu\lambda_{z}^{2}\left(1+2\frac{\partial w}{\partial z}\right)\end{bmatrix}. \tag{19}$$

We can further rewrite Eq. (19) as

$$\frac{\partial u}{\partial x}=\frac{2\sigma_{xx}+2p+\varepsilon E^{2}}{4\mu\lambda_{x}^{2}}-\frac{1}{2}, \tag{20a}$$

$$\frac{\partial v}{\partial y}=\frac{2\sigma_{yy}+2p+\varepsilon E^{2}}{4\mu\lambda_{y}^{2}}-\frac{1}{2}, \tag{20b}$$

$$\frac{\partial w}{\partial z}=\frac{2\sigma_{zz}+2p-\varepsilon E^{2}}{4\mu\lambda_{z}^{2}}-\frac{1}{2}, \tag{20c}$$

$$\lambda_x^2 \frac{\partial v}{\partial x} + \lambda_y^2 \frac{\partial u}{\partial y} = \frac{\sigma_{xy}}{\mu}, \tag{20d}$$

$$\lambda_x^2 \frac{\partial w}{\partial x} + \lambda_z^2 \frac{\partial u}{\partial z} = \frac{\sigma_{xz}}{\mu}, \tag{20e}$$

$$\lambda_y^2 \frac{\partial w}{\partial y} + \lambda_z^2 \frac{\partial v}{\partial z} = \frac{\sigma_{yz}}{\mu}. \tag{20f}$$

The incompressibility condition of the DE film requires that

$$\frac{\partial u}{\partial x} + \frac{\partial v}{\partial y} + \frac{\partial w}{\partial z} = 0. \tag{21}$$

A combination of Eqs. 20 (a-c) and Eq. (21) gives that

$$p = \frac{3\mu\lambda_x^2\lambda_y^2 - \lambda_y^2\sigma_{xx} - \lambda_x^2\sigma_{yy} - \lambda_x^4\lambda_y^4\sigma_{zz} - \lambda_x^4\lambda_y^4\varepsilon E^2}{\lambda_x^2 + \lambda_y^2 + \lambda_x^4\lambda_y^4} - \frac{\varepsilon E^2}{2}. \tag{22}$$

Plugging (22) into 20 (a-f), we can further obtain

$$\frac{\partial u}{\partial x} = \frac{3\mu\lambda_x^2\lambda_y^2 - \lambda_y^2\sigma_{xx} - \lambda_x^2\sigma_{yy} - \lambda_x^4\lambda_y^4\sigma_{zz} - \lambda_x^4\lambda_y^4\varepsilon E^2}{2\mu\lambda_x^2\left(\lambda_x^2 + \lambda_y^2 + \lambda_x^4\lambda_y^4\right)} - \frac{1}{2}, \tag{23a}$$

$$\frac{\partial v}{\partial y} = \frac{3\mu\lambda_x^2\lambda_y^2 - \lambda_x^2\sigma_{yy} - \lambda_y^2\sigma_{xx} - \lambda_x^4\lambda_y^4\sigma_{zz} - \lambda_x^4\lambda_y^4\varepsilon E^2}{2\mu\lambda_y^2\left(\lambda_x^2 + \lambda_y^2 + \lambda_x^4\lambda_y^4\right)} - \frac{1}{2}, \tag{23b}$$

$$\frac{\partial w}{\partial z} = \frac{3\mu\lambda_x^4\lambda_y^4 - \lambda_x^2\lambda_y^4\sigma_{xx} - \lambda_x^4\lambda_y^2\sigma_{yy} - \lambda_x^2\lambda_y^2\left(\lambda_x^2 + \lambda_y^2\right)\sigma_{zz} - \lambda_x^6\lambda_y^6\varepsilon E^2}{2\mu\left(\lambda_x^2 + \lambda_y^2 + \lambda_x^4\lambda_y^4\right)} - \frac{\lambda_x^2\lambda_y^2\varepsilon E^2}{2\mu} - \frac{1}{2}, \tag{23c}$$

$$\lambda_x^2 \frac{\partial v}{\partial x} + \lambda_y^2 \frac{\partial u}{\partial y} = \frac{\sigma_{xy}}{\mu}, \tag{23d}$$

$$\lambda_x^2 \frac{\partial w}{\partial x} + \lambda_z^2 \frac{\partial u}{\partial z} = \frac{\sigma_{xz}}{\mu}, \tag{23e}$$

$$\lambda_y^2 \frac{\partial w}{\partial y} + \lambda_z^2 \frac{\partial v}{\partial z} = \frac{\sigma_{yz}}{\mu}. \tag{23f}$$

A combination of Eqs. (23a-f) and force balance equations gives a complete set of governing equations for both additional displacement field and stress field in a DE. However, without further simplifications, these equations are very difficult to be solved. As discussed previously, in this article, we only focus on additional bending deformation in a DE film, so we will follow Kirchhoff's hypotheses (Ventsel and Krauthammer, 2001) to further simplify the problem. Kirchhoff's hypotheses developed for linear plate theory state that the straight lines, initially normal to the middle plane of a plate before bending, remain straight and normal to the middle surface during bending, and the length of such plate elements does not change. Mathematically, we have the following equations:

$$\frac{\partial w}{\partial z} = 0, \tag{24a}$$

$$\frac{\partial w}{\partial x} + \frac{\partial u}{\partial z} = 0, \tag{24b}$$

$$\frac{\partial w}{\partial y} + \frac{\partial v}{\partial z} = 0. \tag{24c}$$

The three new equations (24a-c) originating from Kirchhoff's hypotheses make the problem overdetermined. Therefore, it is necessary to drop three equations. Following conventional linear plate theory (Ventsel and Krauthammer, 2001), Eqs. (23c, e, f) are discarded. Moreover, the stress normal to the middle plane of the plate is assumed to be negligible comparing with other stress components, i.e. $\sigma_{zz} = 0$. Finally, the nonzero stress components in the DE film can be expressed as

$$\begin{Bmatrix}\sigma_{xx}\\ \sigma_{yy}\\ \sigma_{xy}\end{Bmatrix}=\begin{Bmatrix}\mu\left(\lambda_x^2-\lambda_x^{-2}\lambda_y^{-2}\right)-\varepsilon E^2\\ \mu\left(\lambda_y^2-\lambda_x^{-2}\lambda_y^{-2}\right)-\varepsilon E^2\\ 0\end{Bmatrix}+\begin{Bmatrix}2\mu\left(\lambda_x^{-2}\lambda_y^{-2}+\lambda_x^2\right)\dfrac{\partial u}{\partial x}+2\mu\lambda_x^{-2}\lambda_y^{-2}\dfrac{\partial v}{\partial y}\\ 2\mu\left(\lambda_x^{-2}\lambda_y^{-2}+\lambda_y^2\right)\dfrac{\partial v}{\partial y}+2\mu\lambda_x^{-2}\lambda_y^{-2}\dfrac{\partial u}{\partial x}\\ \mu\left(\lambda_x^2\dfrac{\partial v}{\partial x}+\lambda_y^2\dfrac{\partial u}{\partial y}\right)\end{Bmatrix}. \tag{25}$$

Integrating Eqs. (24a-c), we can obtain the displacement of a material point in the DE film with distance z from the middle plane:

$$\begin{Bmatrix}u_x^z\\ u_y^z\end{Bmatrix}=\begin{Bmatrix}-z\dfrac{\partial w}{\partial x}\\ -z\dfrac{\partial w}{\partial y}\end{Bmatrix}, \tag{26}$$

where $w=w(x,y)$ is independent on z and denotes the deflection of the DE film.

Inserting Eq. (26) into (25), we can further obtain the stress components of a material point in the DE film with distance z from the middle plane

$$\begin{Bmatrix}\sigma_{xx}^z\\ \sigma_{yy}^z\\ \sigma_{xy}^z\end{Bmatrix}=\begin{Bmatrix}\mu\left(\lambda_x^2-\lambda_x^{-2}\lambda_y^{-2}\right)-\varepsilon E^2\\ \mu\left(\lambda_y^2-\lambda_x^{-2}\lambda_y^{-2}\right)-\varepsilon E^2\\ 0\end{Bmatrix}-z\begin{bmatrix}C_{11}&C_{12}&0\\ C_{21}&C_{22}&0\\ 0&0&2C_{66}\end{bmatrix}\begin{Bmatrix}\dfrac{\partial^2 w}{\partial x^2}\\ \dfrac{\partial^2 w}{\partial y^2}\\ \dfrac{\partial^2 w}{\partial x\partial y}\end{Bmatrix}, \tag{27}$$

where $C_{11}=2\mu\left(\lambda_x^{-2}\lambda_y^{-2}+\lambda_x^2\right)$, $C_{22}=2\mu\left(\lambda_x^{-2}\lambda_y^{-2}+\lambda_y^2\right)$, $C_{12}=C_{21}=2\mu\lambda_x^{-2}\lambda_y^{-2}$, $2C_{66}=\mu\left(\lambda_x^2+\lambda_y^2\right)$.

Following the "hypothesis of straight normal", the electrical field in Eq. (27) does not change during bending. The bending moments: M_{xx}, M_{yy} and twisting moment M_{xy} can be integrated as:

$$\begin{Bmatrix} M_{xx} \\ M_{yy} \\ M_{xy} \end{Bmatrix} = \int_{-h/2}^{h/2} \begin{Bmatrix} \sigma_{xx}^{z} \\ \sigma_{yy}^{z} \\ \sigma_{xy}^{z} \end{Bmatrix} z dz = -\frac{H^3}{12\lambda_x^3\lambda_y^3} \begin{bmatrix} C_{11} & C_{12} & 0 \\ C_{21} & C_{22} & 0 \\ 0 & 0 & 2C_{66} \end{bmatrix} \begin{Bmatrix} \dfrac{\partial^2 w}{\partial x^2} \\ \dfrac{\partial^2 w}{\partial y^2} \\ \dfrac{\partial^2 w}{\partial x \partial y} \end{Bmatrix} \quad . \tag{28}$$

In a polar coordinate, the bending moment and twisting moment can be similarly written as:

$$\begin{Bmatrix} M_{rr} \\ M_{\theta\theta} \\ M_{r\theta} \end{Bmatrix} = -\frac{H^3}{12\lambda_r^3\lambda_\theta^3} \begin{bmatrix} C_{rr} & C_{r\theta} & 0 \\ C_{\theta r} & C_{\theta\theta} & 0 \\ 0 & 0 & 2C_{ss} \end{bmatrix} \begin{Bmatrix} \dfrac{\partial^2 w}{\partial r^2} \\ \dfrac{1}{r}\dfrac{\partial w}{\partial r} + \dfrac{1}{r^2}\dfrac{\partial^2 w}{\partial \theta^2} \\ \dfrac{1}{r}\dfrac{\partial^2 w}{\partial r \partial \theta} - \dfrac{1}{r^2}\dfrac{\partial w}{\partial \theta} \end{Bmatrix} , \tag{29}$$

where $C_{rr} = 2\mu\left(\lambda_r^{-2}\lambda_\theta^{-2} + \lambda_r^2\right)$, $C_{\theta\theta} = 2\mu\left(\lambda_r^{-2}\lambda_\theta^{-2} + \lambda_\theta^2\right)$, $C_{r\theta} = C_{\theta r} = 2\mu\lambda_r^{-2}\lambda_\theta^{-2}$, and $2C_{ss} = \mu\left(\lambda_r^2 + \lambda_\theta^2\right)$. Therefore, in a polar coordinate, we have

$$M_{rr} = -\left[D_{rr}\frac{\partial^2 w}{\partial r^2} + D_{r\theta}\left(\frac{1}{r}\frac{\partial w}{\partial r} + \frac{1}{r^2}\frac{\partial^2 w}{\partial \theta^2}\right)\right], \tag{30a}$$

$$M_{\theta\theta} = -\left[D_{\theta\theta}\left(\frac{1}{r}\frac{\partial w}{\partial r} + \frac{1}{r^2}\frac{\partial^2 w}{\partial \theta^2}\right) + D_{\theta r}\frac{\partial^2 w}{\partial r^2}\right], \tag{30b}$$

$$M_{r\theta} = M_{\theta r} = -2D_{ss}\left(\frac{1}{r}\frac{\partial^2 w}{\partial r \partial \theta} - \frac{1}{r^2}\frac{\partial w}{\partial \theta}\right), \tag{30c}$$

where $D_{rr} = \mu H^3\left(\lambda_r^{-5}\lambda_\theta^{-5} + \lambda_r^{-1}\lambda_\theta^{-3}\right)/6$, $D_{\theta\theta} = \mu H^3\left(\lambda_r^{-5}\lambda_\theta^{-5} + \lambda_r^{-3}\lambda_\theta^{-1}\right)/6$, $D_{r\theta} = D_{\theta r} = \mu H^3\lambda_r^{-5}\lambda_\theta^{-5}/6$, and $D_{ss} = \mu H^3\left(\lambda_r^{-1}\lambda_\theta^{-3} + \lambda_r^{-3}\lambda_\theta^{-1}\right)/24$.

In the normal direction, force balance condition requires that

$$\frac{\partial^2 M_{rr}}{\partial r^2}+\frac{2}{r}\frac{\partial M_{rr}}{\partial r}+\frac{2}{r}\frac{\partial^2 M_{r\theta}}{\partial r\partial\theta}+\frac{2}{r^2}\frac{\partial M_{r\theta}}{\partial\theta}-\frac{1}{r}\frac{\partial M_{\theta\theta}}{\partial r}+\frac{1}{r^2}\frac{\partial^2 M_{\theta\theta}}{\partial\theta^2}$$
$$+N_{rr}\frac{\partial^2 w}{\partial r^2}+2N_{r\theta}\left(\frac{1}{r}\frac{\partial^2 w}{\partial r\partial\theta}-\frac{1}{r^2}\frac{\partial w}{\partial\theta}\right)+N_{\theta\theta}\left(\frac{1}{r}\frac{\partial w}{\partial r}+\frac{1}{r^2}\frac{\partial^2 w}{\partial\theta^2}\right)=0, \tag{31}$$

where $N_{rr}=\sigma_{rr}h$, $N_{\theta\theta}=\sigma_{\theta\theta}h$, $N_{r\theta}=\sigma_{r\theta}h$ are the membrane forces.

On the inner circular boundary, the DE film is clamped, namely,

$$w=0, \tag{32}$$

$$\frac{\partial w}{\partial r}=0. \tag{33}$$

On the outer circular boundary, the bending moment is zero and vertical shear force is zero, namely,

$$M_{rr}=0, \tag{34}$$

$$\frac{\partial M_{rr}}{\partial r}+\frac{2}{r}\frac{\partial M_{r\theta}}{\partial\theta}+\frac{M_{rr}-M_{\theta\theta}}{r}=0. \tag{35}$$

A combination of Eqs. (30a-c) and (31) with boundary conditions Eqs. (32)-(35) sets an eigenvalue problem. We assume the deflection of the DE film follows

$$w=Bf(\bar{r})\cos(k\theta), \tag{36}$$

where $\bar{r}=r/B$, $f(\bar{r})$ is a dimensionless single variable function, and k is wavenumber of wrinkle.

Inserting (36) into (30) and (31), we get the following homogeneous ODE,

$$\left(\frac{d^4f}{d\bar{r}^4}+\frac{2}{\bar{r}}\frac{d^3f}{d\bar{r}^3}\right)\overline{D}_{rr}+2\left(\frac{d^3f}{d\bar{r}^3}+\frac{1}{\bar{r}}\frac{d^2f}{d\bar{r}^2}\right)\frac{d\overline{D}_{rr}}{d\bar{r}}+\frac{d^2f}{d\bar{r}^2}\frac{d^2\overline{D}_{rr}}{d\bar{r}^2}+\frac{1}{\bar{r}^2}\left(\frac{1}{\bar{r}}\frac{df}{d\bar{r}}-\frac{d^2f}{d\bar{r}^2}+\frac{k^2-2}{\bar{r}^2}k^2f\right)\overline{D}_{\theta\theta}$$
$$-\frac{1}{\bar{r}^2}\left(\frac{df}{d\bar{r}}-\frac{k^2f}{\bar{r}}\right)\frac{d\overline{D}_{\theta\theta}}{d\bar{r}}+\frac{2k^2}{\bar{r}^2}\left(-\frac{f}{\bar{r}^2}+\frac{1}{\bar{r}}\frac{df}{d\bar{r}}-\frac{d^2f}{d\bar{r}^2}\right)\overline{D}_{r\theta}+\frac{2k^2}{\bar{r}^2}\left(\frac{f}{\bar{r}}-\frac{df}{d\bar{r}}\right)\frac{d\overline{D}_{r\theta}}{d\bar{r}}$$
$$+\frac{1}{\bar{r}}\left(-\frac{k^2f}{\bar{r}}+\frac{df}{d\bar{r}}\right)\frac{d^2\overline{D}_{r\theta}}{d\bar{r}^2}+\frac{4k^2}{\bar{r}^2}\left(-\frac{f}{\bar{r}^2}+\frac{1}{\bar{r}}\frac{df}{d\bar{r}}-\frac{d^2f}{d\bar{r}^2}\right)\overline{D}_{ss}+\frac{4k^2}{\bar{r}^2}\left(\frac{f}{\bar{r}}-\frac{df}{d\bar{r}}\right)\frac{d\overline{D}_{ss}}{d\bar{r}}$$
$$-\frac{12}{\overline{H}^2\lambda_r\lambda_\theta}\left[\overline{\sigma}_{rr}\frac{d^2f}{d\bar{r}^2}+\frac{\overline{\sigma}_{\theta\theta}}{\bar{r}}\left(\frac{df}{d\bar{r}}-\frac{k^2f}{\bar{r}}\right)\right]=0. \tag{37}$$

The corresponding homogeneous boundary conditions are:

$$f\Big|_{\bar{r}=\frac{A}{B}}=0, \tag{38a}$$

$$\frac{df}{d\bar{r}}\Big|_{\bar{r}=\frac{A}{B}}=0, \tag{38b}$$

$$\left[\overline{D}_{rr}\frac{d^2f}{d\bar{r}^2}+\overline{D}_{r\theta}\left(\frac{1}{\bar{r}}\frac{df}{d\bar{r}}-\frac{k^2}{\bar{r}^2}f\right)\right]\Big|_{\bar{r}=\frac{b}{B}}=0, \tag{38c}$$

$$\left[\left(\frac{1}{\bar{r}}\frac{d^2f}{d\bar{r}^2}+\frac{d^3f}{d\bar{r}^3}\right)\overline{D}_{rr}+\frac{1}{\bar{r}^2}\left(\frac{f}{\bar{r}}-\frac{df}{d\bar{r}}\right)\overline{D}_{\theta\theta}+\frac{k^2}{\bar{r}^2}\left(\frac{f}{\bar{r}}-\frac{df}{d\bar{r}}\right)\overline{D}_{r\theta}\right.$$
$$\left.+\frac{4k^2}{\bar{r}^2}\left(\frac{f}{\bar{r}}-\frac{df}{d\bar{r}}\right)\overline{D}_{ss}+\left(-\frac{k^2f}{\bar{r}^2}+\frac{f}{\bar{r}}\frac{df}{d\bar{r}}\right)\frac{d\overline{D}_{r\theta}}{d\bar{r}}+\frac{d^2f}{d\bar{r}^2}\frac{d\overline{D}_{rr}}{d\bar{r}}\right]\Big|_{\bar{r}=\frac{b}{B}}=0. \tag{38d}$$

In Eqs. (37) and (38), we define the following dimensionless quantities: dimensionless thickness: $\overline{H}=H/B$; dimensionless membrane stresses: $\overline{\sigma}_{rr}=\sigma_{rr}/\mu$ and $\overline{\sigma}_{\theta\theta}=\sigma_{\theta\theta}/\mu$; dimensionless bending/twisting stiffness: $\overline{D}_{rr}=2\left(\lambda_r^{-5}\lambda_\theta^{-5}+\lambda_r^{-1}\lambda_\theta^{-3}\right)$, $\overline{D}_{\theta\theta}=2\left(\lambda_r^{-5}\lambda_\theta^{-5}+\lambda_r^{-3}\lambda_\theta^{-1}\right)$, $\overline{D}_{r\theta}=2\lambda_r^{-5}\lambda_\theta^{-5}$, $\overline{D}_{ss}=\left(\lambda_r^{-1}\lambda_\theta^{-3}+\lambda_r^{-3}\lambda_\theta^{-1}\right)/2$. In the equations above, dimensionless thickness $\overline{H}$ and the ratio between inner radius and outer radius of the annular DE film A/B are the only two system parameters which can be varied in experiments. The membrane stresses in the radial and hoop directions: $\overline{\sigma}_{rr}$ and $\overline{\sigma}_{\theta\theta}$, and the bending/twisting stiffness both depend on the electrical field E or

voltage Φ, which can be regarded as loading parameters for the system. For a given set of parameters: $\overline{H}$ and A/B, we can solve the eigenvalue problem in Eq. (37) with boundary conditions (38) numerically by using the function *bvp4c* in Matlab. The characteristic equation determines the critical condition, namely voltage, for the onset of wrinkles, and the associated eigenvectors give the mode of wrinkling.

4. Results and discussions

Using shooting method, we solve the ODEs of Eqs. (7) and (8) associated with the boundary conditions (9) and (10) for a constrained annular DE film without wrinkle formation. Fig. 3 plots the distributions of radial stretch and hoop stretch in the annular DE film, for several different voltages and ratios between inner and outer radius of the film. With increasing the voltage, both radial stretch and hoop stretch increases.

As shown in Fig. 3, when the voltage is larger than a critical value, no equilibrium solution can be found, which corresponds to pull-in instability of the DE film. Pull-in instability is one of the most important electromechanical failure modes in DE structures (Zhao and Suo, 2007; Norris, 2008; Zhou et al., 2008). The critical voltage for the pull-in instability increases with the increase the ratio A/B as plotted in Fig. 4. When the ratio A/B approaches zero, the annular DE film behaves like a free-standing film. It has been shown in previous studies that the critical voltage for the pull-in instability of a free-standing neo-Hookean DE film is $\Phi_{\text{pull-in}}/\left(H\sqrt{\mu/\varepsilon}\right)=0.69$ (Zhao and Suo, 2007). When the ratio A/B approaches one,

the deformation state in the annular DE film is close to pure-shear. It can also be easily shown that for a DE film with voltage-induced pure-shear deformation, the normalized voltage for pull-in instability is: $\Phi_{\text{pull-in}}/\left(H\sqrt{\mu/\varepsilon}\right)=1$. Both two limiting scenarios discussed above have been plotted in Fig. 4.

Fig. 5 plots the distribution of radial stress and hoop stress in the annular DE film without wrinkle formation for several different radius ratios and applied voltages. The results show that the radial stress in the DE film is tensile, while the hoop stress in the film is compressive. For a given radius ratio, both radial stress and hoop stress in the DE film increase with increasing the voltage. In addition, the radial stress in the DE film monotonically decreases from the inner boundary to the outer boundary as shown in Figs. 5a, c and e. The distribution of the hoop stress is little bit more intricate. For small radius ratio, the hoop stress in the DE film monotonically increases from the inner boundary to outer boundary. However, for big radius ratio, the hoop stress in the DE film may monotonically decrease from the inner boundary to the outer boundary when the voltage is large as shown in Fig. 5f.

When the voltage is high enough, compressive hoop stress can induce wrinkles in the annular DE film as shown in our experiments (Fig. 1). By solving the eigenvalue problem formulated in *Section 3*, we can calculate the critical voltage for the onset of wrinkles with different wavelength in the DE film for different values of A/B. Our calculation results are plotted in Fig. 6. For a given value of A/B and wavenumber k of wrinkles, the voltage for the onset of wrinkles decreases with decreasing the thickness of the film, namely, H/B. The results suggest that lower voltage is needed to

trigger wrinkle formation in thinner DE films. For different values of A/B, the wrinkling mode which needs the lowest critical voltage is also different. For instance, in Fig. 6a, for A/B=0.1, the wrinkling mode with k=2 needs the lowest voltage; in Fig. 6b, for A/B=0.3, the critical mode is k=3. Figs. 6c and d show that the critical modes are k=4 and k=6 or 7 for A/B=0.5 and 0.7, respectively. In Figs. 6a-d, we also plot the voltage for inducing pull-in instability in the DE film. For a thick DE film, the critical voltage for wrinkling may be even larger than the critical voltage for pull-in instability. Therefore, for thick DE films, the wrinkles form after pull-in instability, which can be consequently regarded as an indication of material failure.

In Fig. 7, we plot the dependence of critical wrinkling mode on the ratio between the inner radius and outer radius of the DE film for two different film thicknesses: H/B=0.02 and 0.005, respectively. The result shows that the wavenumber of the critical wrinkling mode increases with increasing the value of A/B. The trend agrees well with the wrinkling instability observed in a constrained annular film induced by differential swelling or plastic deformation (Mora and Boudaoud, 2006; Coman and Bassom, 2007). The results also show that for a given radius ratio, the DE film with different thickness may also have different critical wrinkling mode. For the ratio: A/B=0.75, the critical wrinkling mode of the DE film with thickness: H/B=0.02 *is* k=7 while k=8 for the film with H/B=0.005.

In the experiment, it is usually challenging to precisely measure the critical voltage for the onset of wrinkles in a DE film. However, the wavenumber of wrinkles in the DE film can be easily measured as shown in Fig. 1. The experimental results of

the wavenumber of wrinkles in annular DE films for three different values of A/B are plotted together with our predictions as shown in Fig. 7. The wavenumber of wrinkles in the experiments are consistently larger than the predictions. This difference can be understood as follows: as described in *section 2* and also shown in Fig. 1, to avoid electrical arcing, a gap near the free edge of the annular DE film is intentionally not coated by electrode. Due to the additional constraint from the gap which is not considered in our model, stretching free energy penalty (compared to bending energy penalty) in the film is actually larger than the prediction. Therefore, in the experiments, wavenumber of wrinkles in the film is larger than predictions to reduce stretching energy penalty.

Based on our calculation, we construct a phase diagram for a constrained DE annular film with the thickness H/B=0.02 as shown in Fig. 8. Depending on the radius ratio and magnitude of voltage, the DE film may stay in one of the three phases: flat, wrinkling and pull-in instability. It can be seen from Fig. 8 that the critical voltage for triggering wrinkling in the DE film first decreases and then increases with increasing the ratio between inner radius and outer radius. When A/B=0.4, the required voltage to induce wrinkles in the film is the lowest.

5. Conclusions

In this paper, we formulate a linear plate theory for a DE film under electromechanical loading with small three deformation field superposed onto a finite two dimensional deformation. Based on the theory, we investigate the

formation and morphology of wrinkles in an annular DE film subjected to a voltage and clamped on its inner radius. The theoretical predictions of wrinkling in the DE film agree well with our experimental observations. Furthermore, we show that for certain ranges of ratio between inner radius and outer radius of the DE film, the critical voltage of inducing pull-instability of the system can be lower than the critical voltage of inducing wrinkles in the film. As a result, we construct a phase diagram with three different regions depending on the magnitude of voltage and the ratio between inner radius and outer radius of an annular DE film: 1 the region corresponding to stable and flat configuration of the film; 2 wrinkling region; 3 the region for pull-in instability. The results obtained in the paper and the methodology developed here will be useful for the future design of DE structures.

Acknowledgements

Kai Li acknowledges the supports from Chinese Natural Science Foundation (Grant Nos. 11402001 and 11472005), and Anhui Provincial Natural Science Foundation (Grant No. 1408085QA18). Shengqiang Cai acknowledges the funds from National Science Foundation through Grant No. CMMI-1538137.

References

Anderson, I.A., Hale, T., Gisby, T., Inamura, T., McKay, T., O' Brien, B., Walbran, S., Calius, E.P., 2010. A thin membrane artificial muscle rotary motor. Appl. Phys. A 98 (1), 75-83.

Bertoldi, K., Gei, M., 2011. Instabilities in multilayered soft dielectrics. J. Mech. Phys. Solids 59 (1), 18-42.

Brochu, P., Pei, Q.B., 2010. Advances in dielectric elastomers for actuators and artificial muscles. Macromol. Rapid Commun. 31, 10–36.

Carpi, F., De Rossi, D., Kornbluh, R., Pelrine, R., Sommer-Larsen, P., 2008. Dielectric Elastomers as Electromechanical Transducers. Elsevier, Oxford, UK.

Coman, C.D., Bassom, A.P., 2007. On the wrinkling of a pre-stressed annular thin film in tension. J. Mech. Phys. Solids 55 (8), 1601-1617.

Conn, A.T., Rossiter, J., 2012. Harnessing electromechanical membrane wrinkling for actuation. Appl. Phys. Lett. 101 (17), 171906.

Davidovitch, B., Schroll, R.D., Vella, D., Adda-Bedia, M., Cerda, E.A., 2011. Prototypical model for tensional wrinkling in thin sheets. Proc. Natl. Acad. Sci. USA 108 (45), 18227-18232.

De Tommasi, D., Puglisi, G., Zurlo, G., 2011. Compression-induced failure of electroactive polymeric thin films. Appl. Phys. Lett. 98 (12), 123507.

De Tommasi, D., Puglisi, G., Zurlo, G., 2013a. Electromechanical instability and oscillating deformations in electroactive polymer films. Appl. Phys. Lett. 102 (1),

011903.

De Tommasi, D., Puglisi, G., Zurlo, G., 2013b. Inhomogeneous deformations and pull-in instability in electroactive polymeric films. Int. J. Nonlin. Mech. 57, 123-129.

De Tommasi, D., Puglisi, G., Zurlo, G., 2014. Failure modes in electroactive polymer thin films with elastic electrodes. J. Phys. D Appl. Phys. 47 (6), 065502.

Dervaux, J., Amar, M.B., 2008. Morphogenesis of growing soft tissues. Phys. Rev. Lett. 101 (6), 068101.

Díaz-Calleja, R., Llovera-Segovia, P., Dominguez, J.J., Rosique, M.C., Lopez, A.Q., 2013. Theoretical modelling and experimental results of electromechanical actuation of an elastomer. J. Phys. D Appl. Phys. 46 (23), 235305.

Diaz-Calleja, R., Llovera-Segovia, P., Quijano-López, A., 2014. Bifurcations in biaxially stretched highly non-linear materials under normal electric fields. Europhys. Lett. 108 (2), 26002.

Dorfmann, A., Ogden, R.W., 2005. Nonlinear electroelasticity. Acta Mech. 174, 167–183.

Dorfmann, L., Ogden, R.W., 2014. Instabilities of an electroelastic plate. Inter. J. Eng. Sci. 77, 79-101.

Goulbourne, N.C., Mockensturm, E.M., Frecker, M.I., 2005. A nonlinear model for dielectric elastomer membranes. ASME J. Appl. Mech. 72, 899–906.

Huang, R., Suo, Z.G., 2012. Electromechanical phase transition in dielectric elastomers. Proc. R. Soc. A 468, 1014–1040.

Keplinger, C., Sun, J.Y., Foo, C.C., Rothemund, P., Whitesides, G.M., Suo, Z.G., 2013.

Stretchable, transparent, ionic conductors. Science 341 (6149), 984-987.

Kollosche, M., Kofod, G., Suo, Z.G., Zhu, J., 2015. Temporal evolution and instability in a viscoelastic dielectric elastomer. J. Mech. Phys. Solids 76, 47-64.

Kornbluh, R.D., Pelrine, R., Prahlad, H., Wong-Foy, A., McCoy, B., Kim, S., Eckerle, J., Low, T., 2012a. From boots to buoys: promises and challenges of dielectric elastomer energy harvesting. In: Electroactivity in Polymeric Materials. Springer, US.

Kornbluh, R.D., Pelrine, R., Prahlad, H., Wong-Foy, A., McCoy, B., Kim, S., Eckerle, J., Low, T., 2012b. Dielectric elastomers: stretching the capabilities of energy harvesting. MRS Bull. 37, 246–253.

Li, T.F., Keplinger, C., Baumgartner, R., Bauer, S., Yang, W., Suo, Z.G., 2013. Giant voltage-induced deformation in dielectric elastomers near the verge of snap-through instability. J. Mech. Phys. Solids 61 (2), 611–628.

Liang, X.D., Cai, S.Q., 2015. Shape bifurcation of a spherical dielectric elastomer balloon under the actions of internal pressure and electric voltage. ASME J. Appl. Mech. 82 (10), 101002.

Liu, X., Li, B., Chen, H., Jia, S., Zhou, J., 2016. Voltage-induced wrinkling behavior of dielectric elastomer. J. Appl. Polym. Sci. 133, 43258.

Lu, T., An, L., Li, J., Yuan, C., Wang, T.J., 2015. Electro-mechanical coupling bifurcation and bulging propagation in a cylindrical dielectric elastomer tube. J. Mech. Phys. Solids 85, 160-175.

Mao, G., Huang, X., Diab, M., Li, T., Qu, S., Yang, W., 2015. Nucleation and propagation of voltage-driven wrinkles in an inflated dielectric elastomer

balloon. Soft matter 11 (33), 6569-6575.

McMeeking, R.M., Landis, C.M., 2005. Electrostatic forces and stored energy for deformable dielectric materials. ASME J. Appl. Mech. 72, 581–590.

Mora, T., Boudaoud, A., 2006. Buckling of swelling gels. Euro. Phys. J. E 20 (2), 119-124.

Norris, A.N., 2008. Comment on 'method to analyze electromechanical instability of dielectric elastomers'. Appl. Phys. Lett. 92, 026101.

O'Brien, B., McKay, T., Calius, E., Xie, S., Anderson, I., 2009. Finite element modelling of dielectric elastomer minimum energy structures. Appl. Phys. A 94, 507–514.

O'Halloran, A., O'Malley, F., McHugh, P., 2008. A review on dielectric elastomer actuators, technology, applications, and challenges. J. Appl. Phys. 104, 071101.

Park, H.S., Suo, Z.G., Zhou, J., Klein, P.A., 2012. A dynamic finite element method for inhomogeneous deformation and electromechanical instability of dielectric elastomer transducers. Int. J. Solids Struct. 49 (15), 2187-2194.

Piñeirua, M., Tanaka, N., Roman, B., Bico, J., 2013. Capillary buckling of a floating annulus. Soft Matter 9 (46), 10985-10992.

Plante, J.S., Dubowsky, S., 2006. Large-scale failure modes of dielectric elastomer actuators. Int. J. Solids Struct. 43 (25), 7727–7751.

Shian, S., Bertoldi, K., Clarke, D.R., 2015. Dielectric elastomer based "grippers" for soft robotics. Adv. Mater. 27 (43), 6814-6819.

Shivapooja, P., Wang, Q., Orihuela, B., Rittschof, D., López, G.P., Zhao, X.H., 2013. Bioinspired surfaces with dynamic topography for active control of biofouling. Adv. Mater. 25 (10), 1430-1434.

Suo, Z.G., Zhao, X.H., Greene, W.H., 2008. A nonlinear field theory of deformable dielectrics. J. Mech. Phys. Solids 56, 467–486.

Trimarco, C., 2009. On the dynamics of electromagnetic bodies. Int. J. Adv. Eng. Sci. Appl. Math. 1, 157–162.

Ventsel, E., Krauthammer, T., 2001. Thin Plates and Shells: Theory, Analysis, and Applications. Marcel Dekker Inc., New York.

Vu, D.K., Steinmann, P., Possart, G., 2007. Numerical modelling of non-linear electroelasticity. Int. J. Numer. Methods Eng. 70, 685–704.

Wang, Q., Gossweiler, G.R., Craig, S.L., Zhao, X.H., 2014. Cephalopod-inspired design of electro-mechano-chemically responsive elastomers for on-demand fluorescent patterning. Nat. Commun. 5, 4899.

Wang, Q., Tahir, M., Zhang, L., Zhao, X.H., 2011. Electro-creasing instability in deformed polymers: experiment and theory. Soft Matter 7 (14), 6583-6589.

Xie, Y.X., Liu, J.C., Fu, Y.B., 2016. Bifurcation of a dielectric elastomer balloon under pressurized inflation and electric actuation. Int. J. Solids Struct. 78, 182-188.

Xu, D., Tairych, A., Anderson, I.A., 2015. Localised strain sensing of dielectric elastomers in a stretchable soft-touch musical keyboard. Proc. SPIE 943025.

Zhao, X.H., Suo, Z.G., 2007. Method to analyze electromechanical stability of dielectric elastomers. Appl. Phys. Lett. 91, 061921.

Zhou, J.X., Hong, W., Zhao, X.H., Zhang, Z.Q., Suo, Z.G., 2008. Propagation of instability in dielectric elastomers. Int. J. Solids Struct. 45, 3739–3750.

Zhu, J., Kollosche, M., Lu, T., Kofod, G., Suo, Z.G., 2012. Two types of transitions to wrinkles in dielectric elastomers. Soft Matter 8, 8840–8846.

Zurlo, G., 2013. Non-local elastic effects in electroactive polymers. Int. J. Nonlin. Mech. 56, 115-122.

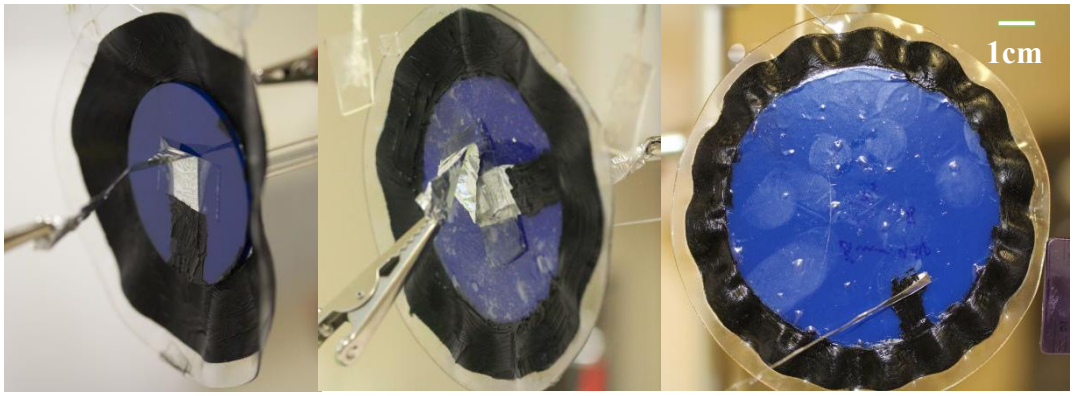

(a) A/B=0.6 (b) A/B=0.7 (c) A/B=0.8

Fig. 1 Experimental photos of voltage-induced wrinkles in a constrained annular DE film with different ratios between the inner radius A and outer radius B. (a) A/B=0.6, (b) A/B=0.7, (c) A/B=0.8. The wavenumber of wrinkling mode increases with increasing radius ratio.

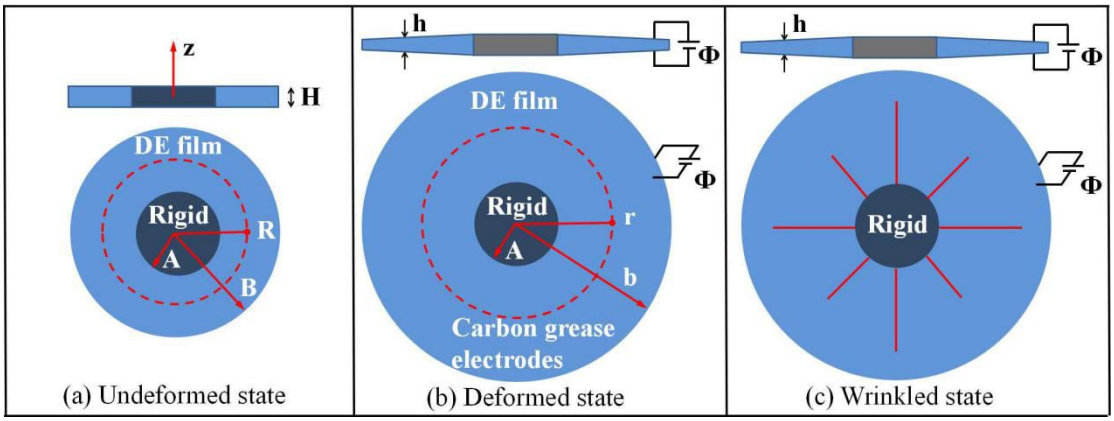

Fig. 2 Schematics of an annular DE film constrained by an inner circular rigid plate. The inner radius and outer radius of the annular DE film without deformation are denoted by A and B, respectively. In the experiment, an electrical voltage Φ is applied across the thickness of the DE film. Three different states of the annular DE film are sketched: (a) undeformed state; (b) deformed state without wrinkles; (c) wrinkled state.

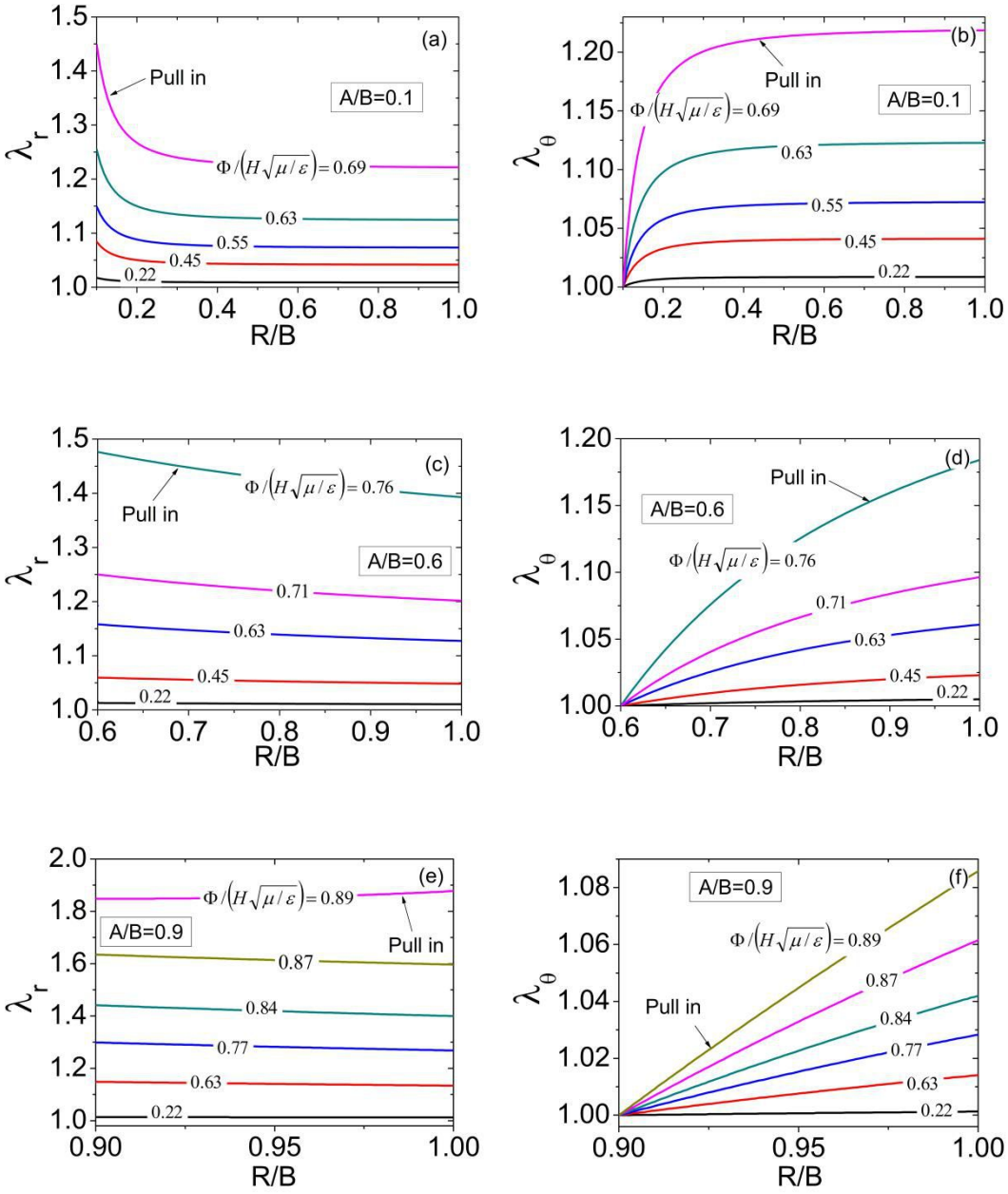

Fig. 3 Distributions of radial stretch and hoop stretch in a constrained annular DE film for several different voltages and ratios between its inner radius *A* and outer radius *B*. The highest voltages in the figures correspond to the critical voltage of inducing pull-in instability in the DE film.

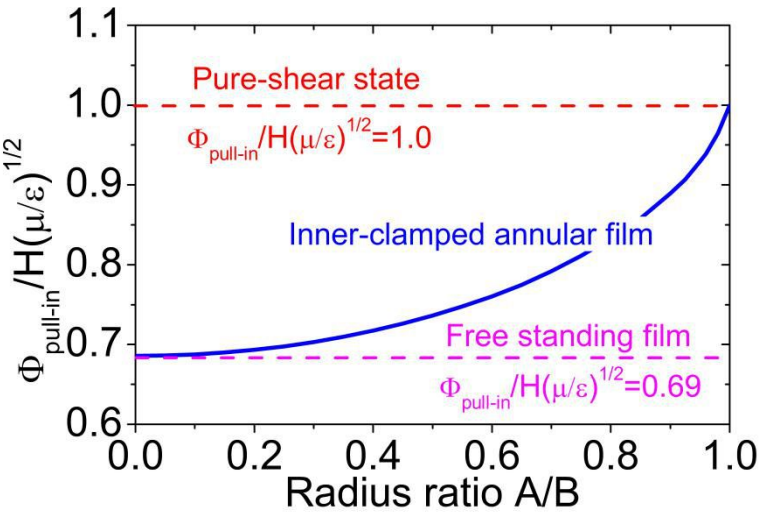

Fig. 4 Dependence of the critical voltage of inducing pull-in instability of the annular DE film on the ratio between its inner radius and outer radius. When the ratio between inner radius and outer radius approaches zero, the annular film becomes a free-standing film; when the ratio approaches one, the deformation state of the film is pure-shear.

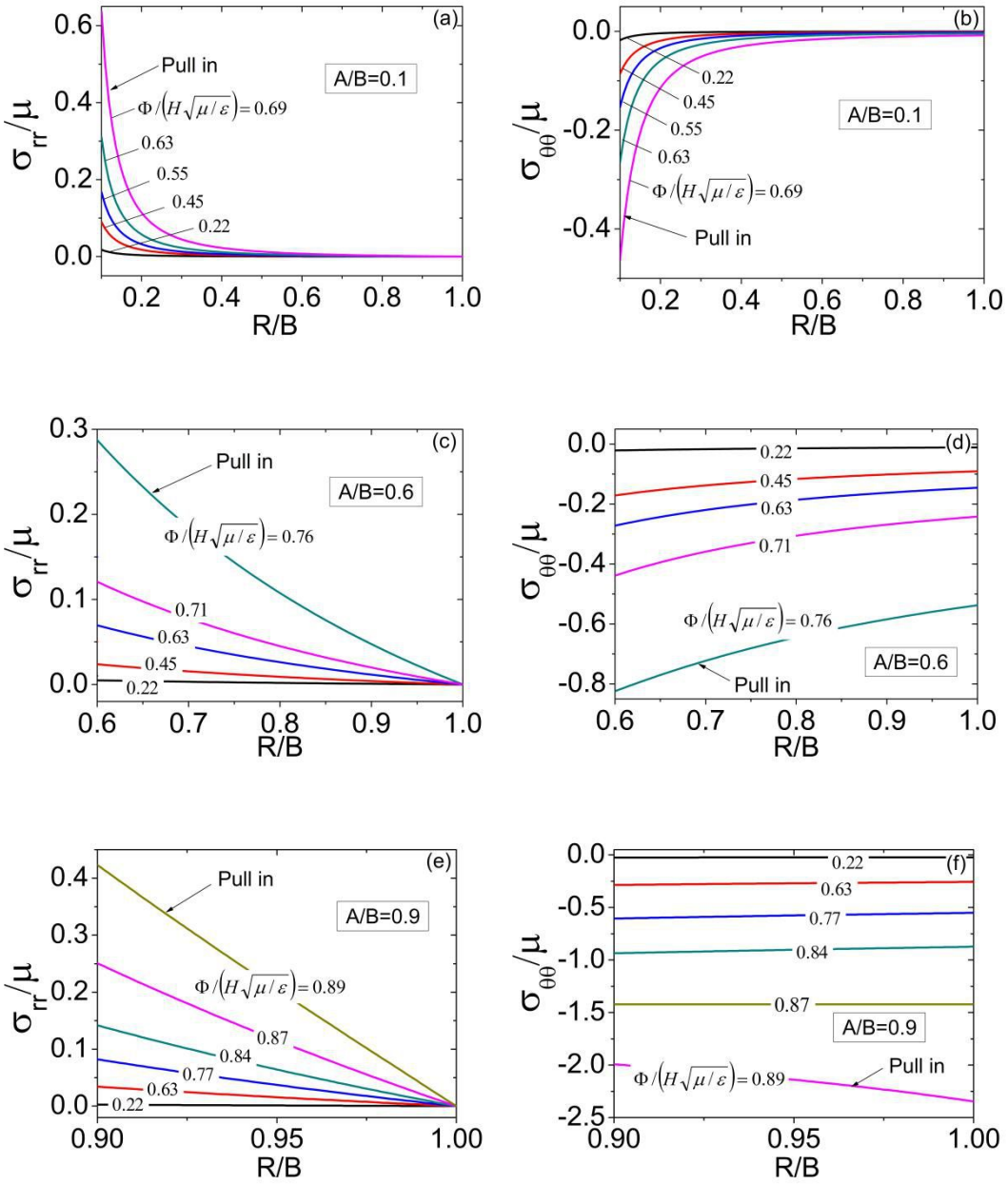

Fig. 5 Distributions of radial stress and hoop stress in the DE film without wrinkles, for several voltages and radius ratios. The radial stress in the film is tensile, while the hoop stress is compressive. The compressive hoop stress may wrinkle the DE film.

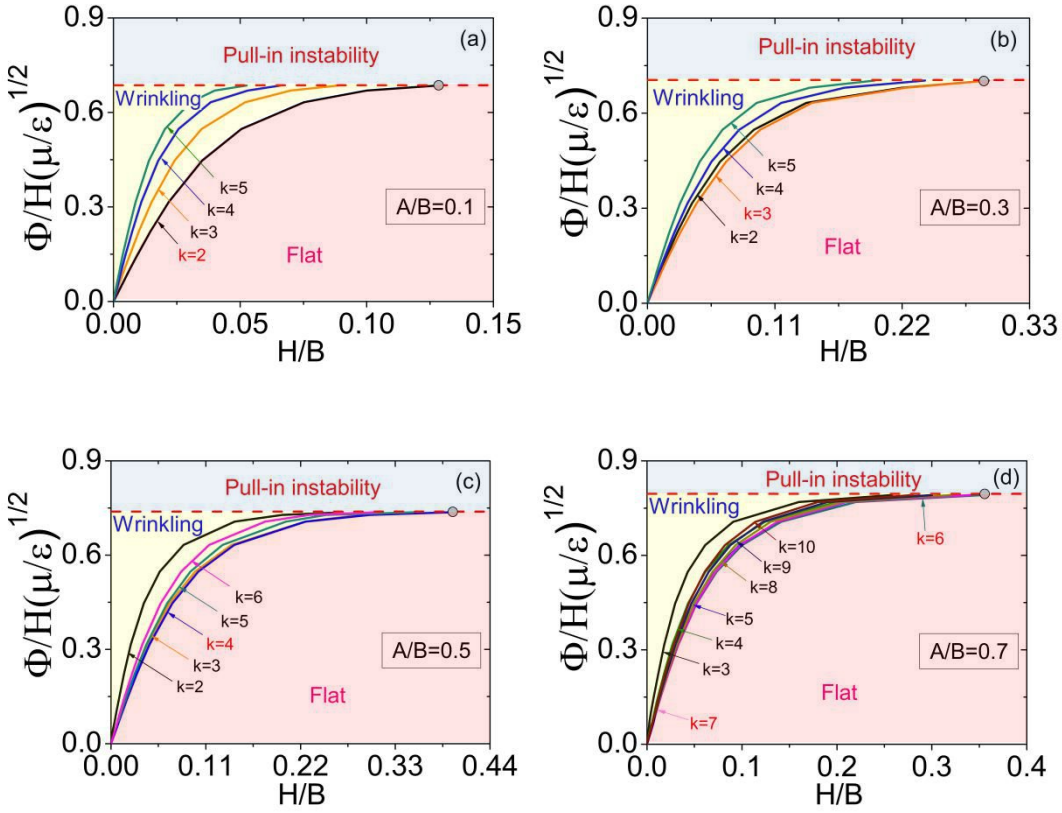

Fig. 6 Dependence of critical voltage for inducing wrinkling instability on the thickness of the DE film, for several radius ratios and wrinkling modes. For large film thickness, the voltage for inducing pull-in instability is smaller than the voltage for inducing wrinkling in the film.

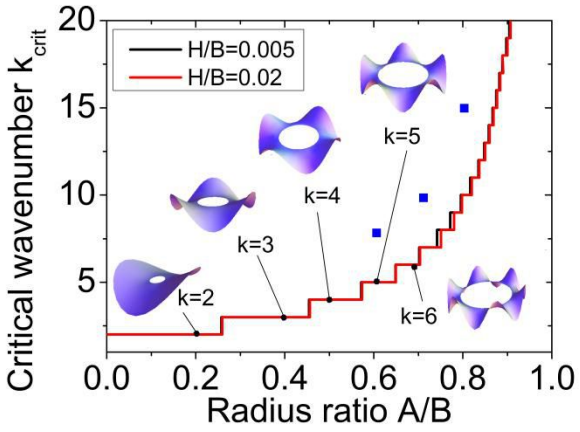

Fig.7 Dependence of the wavenumber of the critical wrinkling mode on the radius ratio for two different film thicknesses H/B=0.02 and 0.005. The three dots are experimental results from Fig. 1.

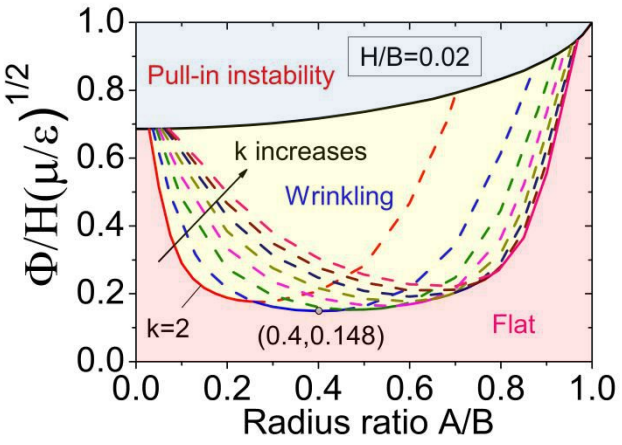

Fig.8 A phase diagram of a constrained annular DE film with thickness H/B=0.02. Depending on the ratio between the inner radius and outer radius of the film and the magnitude of applied voltage, the film may stay in a flat and stable phase, wrinkling phase or pull-in instability phase. The boundary between the flat phase and wrinkling phase of the DE film is given by the dependence of critical voltage for wrinkling on its radius ratio A/B. For the annular DE film with the radius ratio: A/B=0.4, the required voltage to induce wrinkles in the film is the lowest.